

# Helium Volumetric Recombining Plasma Formation for Energetic Ion Injection in Radio-Frequency Plasma Device DT-ALPHA<sup>\*)</sup>

Hiroyuki TAKAHASHI, Atsushi OKAMOTO<sup>1)</sup>, Takatsugu MIURA, Daiki NAKAMURA, Peerapat BOONYARITTIPONG, Shuhei SEKITA and Sumio KITAJIMA

*Department of Quantum Science and Energy Engineering, Tohoku University, Sendai 980-8579, Japan*

<sup>1)</sup>*Department of Energy Engineering and Science, Nagoya University, Nagoya 464-8603, Japan*

(Received 30 November 2015 / Accepted 11 March 2016)

The spatial distribution of helium volumetric recombination in a radio-frequency (RF) plasma device was investigated in two different plasma production cases. It was revealed that the radial distribution of volumetric recombination was strongly localized in the peripheral region of a cylindrical plasma at a higher RF heating power and lower neutral pressure case. In contrast, volumetric recombination was widely distributed around the plasma column at a lower RF heating power and higher neutral pressure. To understand helium recombining plasma formation, the electron-ion temperature relaxation time was evaluated for each plasma production case. The electron-ion temperature relaxation time in the gas puffing region becomes much smaller than the plasma confinement time in the latter plasma production case, whereas it is much larger than the plasma confinement time in the former plasma production case. This result indicates that energy transfer from electrons to bulk ions plays an important role in helium recombining plasma formation in an RF plasma device.

© 2016 The Japan Society of Plasma Science and Nuclear Fusion Research

Keywords: divertor, helium plasma, volumetric recombination, energetic ion injection, electron-ion energy transfer

DOI: 10.1585/pfr.11.2402059

## 1. Introduction

In research on magnetically confined fusion, mitigation of the heat load on plasma-facing components is one of the most crucial issues. Detached divertor operation is a promising candidate for handling the enormous heat load flowing onto the divertor plate because the plasma pressure in a volumetric recombining plasma drops rapidly along the magnetic field lines [1]. Because the reaction rate of volumetric recombination becomes large in regions of low electron temperature and high electron density, typically  $T_e < 1$  eV and  $n_e > 10^{18}$  m<sup>-3</sup>, sufficient plasma-neutral interactions are required for steady-state heat load mitigation by the detached divertor formation. On the other hand, the edge-localized modes associated with high confinement mode (H-mode) plasma bring energetic plasma particles into the divertor region through the scrape-off layer. In next-generation fusion reactors, simultaneous operation of the H-mode plasma and the detached divertor is expected. The energy of the exhausted particles potentially rises to several keV. Therefore, a comprehensive understanding of the detached/recombining plasma dynamics that coexists with transiently transported undesirable energetic particles has been one of the most important subjects in recent divertor plasma studies. Although it has been demonstrated that energetic electrons injected into the helium detached

plasma enhance ionization and excitation [2, 3], the dynamic response, which is provided by ions of several keV, remains ambiguous because conventional divertor plasma simulators have difficulties with energetic ion production.

As described above, another type of divertor plasma simulating device is required to reveal the divertor plasma dynamics induced by energetic ions. A linear plasma machine with a radio-frequency (RF) plasma source is available because a cylindrically wound RF antenna makes it possible to superimpose an energetic ion beam onto a target plasma. The ionization and excitation reaction rates due to energetic ions would be comparable to those for thermal electrons of several eV. Therefore, ionization of ground-state neutral atoms due to energetic ions is expected to be negligible. On the other hand, electrons of even several eV could re-ionize the Rydberg atoms produced by volumetric recombination because the ionization potential of the Rydberg atoms is much smaller than that of the ground-state neutral atoms. Therefore, energetic ions, as well as several eV electrons, have a non-negligible affect on the Rydberg atoms; thus, they could modulate the ionization-recombination balance. Moreover, ions of around several keV have a large cross-section for the charge-exchange interaction, which transfers momentum from the fast ions to bulk neutrals. Therefore, redistribution of the ground-state/excited neutral atoms through the ion intrinsic reaction is concerned. For example, energetic helium ion injection into helium ionizing plasma in-

author's e-mail: [hiroyuki.takahashi@qse.tohoku.ac.jp](mailto:hiroyuki.takahashi@qse.tohoku.ac.jp)

<sup>\*)</sup> This article is based on the presentation at the 25th International Toki Conference (ITC25).

dicates that charge-exchange momentum transfer spatially redistributes neutral atoms [4]. An energetic ion injection experiment requires (1) steady-state production of a detached/recombining plasma and (2) energetic ion beam superimposition onto a target plasma. Although secondary gas puffing is an effective method of inducing volumetric recombination in the target plasma, back-flowing of the neutral atoms is an anticipated difficulty in the RF plasma device. In our previous works, compatibility among stable RF discharge and secondary gas puffing was maintained by introducing orifice units, and helium recombining plasma production in an RF plasma source was achieved [5, 6]. Then an ion beam source was developed to extract energetic helium ions [7]. These advances enabled a divertor-simulating experiment with energetic ion beam injection, and a preliminary result was reported [8]. For a beam injection experiment, the spatial distribution of volumetric recombination is important because energetic ions penetrate through the central region of a cylindrical target plasma. However, the details of helium volumetric recombining plasma formation was not clarified in the above studies. In the present report, helium recombining plasma formation and its spatial distribution in an RF plasma source are reported.

## 2. Experimental Setup

Experiments were performed using the radio-frequency (RF) plasma device DT-ALPHA [9]. Figure 1 shows a schematic of the DT-ALPHA device, which consists of a quartz tube and a stainless steel (SUS) vacuum chamber. The  $y$  and  $z$  axes are defined as illustrated in Fig. 1. At the upstream and downstream ends of the DT-ALPHA device, end-plates are installed, and helium working gas is supplied to the device near the upstream end-plate. Plasma is produced by a 13.56 MHz oscillating field supplied through an RF antenna coupled with the quartz tube and the maximum heating power  $P_{RF}$  is 3 kW. A gas puffing system is introduced at  $z = 1.58$  m to decrease the electron temperature because the typical electron temperature in the DT-ALPHA device is several eV. Between  $z = 0.98$  and 1.58 m, two orifice units made of SUS are installed because back-flowing of the secondary gas becomes a crucial problem for maintaining stable

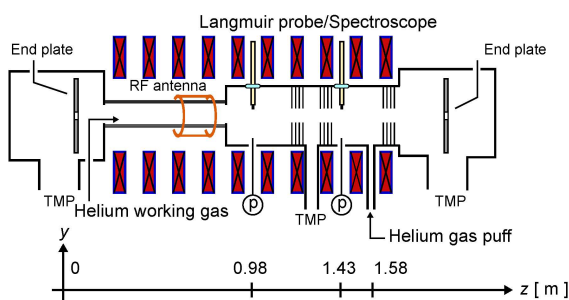


Fig. 1 Schematic of the RF plasma device DT-ALPHA.

RF discharge. The neutral pressure in the test region,  $p_{test}$  ( $z = 1.43 - 1.58$  m), is controlled within a range of below 1 Pa to above 10 Pa by a secondary gas puffing method. The inner diameter of the orifice unit is 20 mm. Thus, the diameter of a cylindrical plasma in the test region is also approximately 20 mm. In this experiment, additional helium gas was supplied to the DT-ALPHA device to form a helium recombining plasma. Magnetic coils equipped around the vacuum chamber produce a converging magnetic field. The magnetic field strengths near the RF antenna and the test region are  $B \sim 0.05, 0.2$  T, respectively.

Plasma diagnostics were performed using Langmuir probes and a spectroscope at the  $z = 0.98, 1.43$  m. In this experiment, the helium volumetric recombining plasma was characterized in two different plasma production cases. The experimental conditions are described in detail in Sec. 3 with the experimental results.

## 3. Experimental Results

The radial distribution of the helium volumetric recombining plasma formed in the test region ( $z = 1.43$  m) was investigated using a Langmuir probe method and optical emission spectroscopy. Plasma diagnostics were performed in two different plasma production condition cases: (1)  $P_{RF} \sim 900$  W,  $p_{test} \sim 4$  Pa (case I) and (2)  $P_{RF} \sim 350$  W,  $p_{test} \sim 6$  Pa (case II). In this section, the results of the spectroscopic measurement are described. The electron temperature and electron density obtained by Langmuir probes are described in Sec. 4.

### 3.1 Higher RF heating power and lower neutral pressure case (case I)

Figure 2 shows a typical wavelength spectrum in the central and peripheral regions of a plasma column ( $y = 0, 10$  mm). Line spectra from the  $2^3P - n^3D$  ( $n = 10 - 14$ ) transitions are clearly observed around  $\lambda = 350$  nm at  $y = 10$  mm. On the other hand, no clear line spectra are ob-

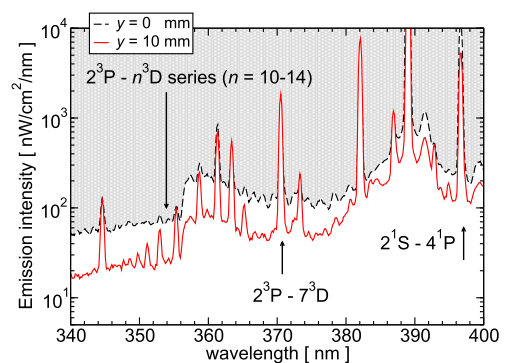


Fig. 2 Typical wavelength spectrum of a helium recombining plasma observed at  $z = 1.43$  m. Dashed and solid lines correspond to the results measured at  $y = 0, 10$  mm, respectively.

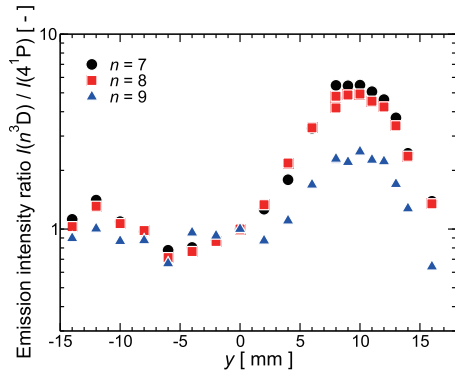


Fig. 3 Radial distribution of the emission intensities from  $2^3\text{P} - n^3\text{D}$  transitions divided by the emission intensity from  $2^1\text{S} - 4^1\text{P}$  transition. Circles, squares, and triangles are correspond to  $n = 7, 8,$  and  $9,$  respectively.

served at  $y = 0$  mm. A Boltzmann plot of the emission intensities from the  $n^3\text{D}$  levels indicates that the electrons of the highly excited helium atoms ( $n \geq 10$ ) are in local thermodynamic equilibrium, and it gives an electron temperature of  $T_e \sim 0.04$  eV. Figure 3 shows the radial distribution of the emission intensity from the  $n^3\text{D}$  levels,  $I(n^3\text{D})$ , divided by that from the  $4^1\text{P}$  level,  $I(4^1\text{P})$ . Here, the vertical axis is normalized by the emission intensity ratio at  $y = 0$  mm. The emission intensity ratio  $I(n^3\text{D})/I(4^1\text{P})$  shows a hollowed radial profile, and it peaks at the edge of the plasma column, especially around  $y = 10$  mm. The population density of highly excited helium atoms as Rydberg atoms is dominated mainly by a recombination process, whereas atoms in lower excited levels, such as the  $4^1\text{P}$  state, are distributed by an ionizing process. Therefore, Fig. 3 is expected to reflect the ionization–recombination balance inside the plasma column. Furthermore, Fig. 3 indicates that volumetric recombination is strongly localized in the peripheral region in this plasma production case.

However, the above results include the line-integration effect. Thus, the local plasma properties were investigated in detail, as described below. First, the local optical emission intensity  $\varepsilon(y)$  was evaluated by a helium collisional-radiative model (CR model) [10, 11] using the electron temperature and electron density obtained by the Langmuir probe. Then, the  $\varepsilon(y)$  obtained at each radial position was integrated toward the line of sight (the Abel transform). Abel transform of  $\varepsilon(y)$  yields the line-integrated emission intensity  $I(y)$ . Note that  $T_e$  and  $n_e$  were obtained discretely as shown in Sec. 4, so the  $\varepsilon(y)$  between two adjacent measurement positions were extrapolated assuming linearity. The results of the Abel transform are shown in Fig. 4, which shows the radial profile of the experimentally observed emission intensities (circles) and the Abel transform of  $\varepsilon(y)$  (solid and dashed lines). Here, emission from the  $4^1\text{P}$  and  $7^3\text{D}$  levels is used for comparison because atoms in the  $4^1\text{P}$  level have the lowest principal quantum number among several emission lines that were simultaneously observed in a single spectroscopic measurement. Further, the

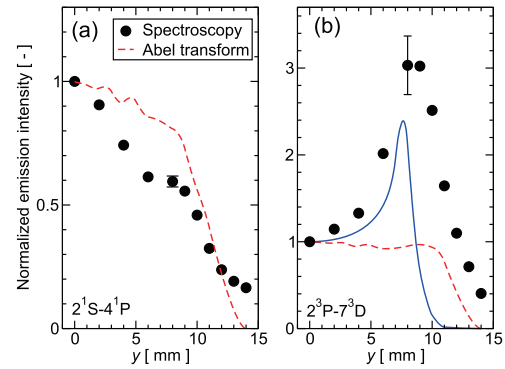


Fig. 4 Radial distribution of the experimentally obtained emission intensities (circles) from (a)  $2^1\text{S} - 4^1\text{P}$  transition and (b)  $2^3\text{P} - 7^3\text{D}$  transition. Solid and dashed lines are Abel transform of the local emission intensity  $\varepsilon(y)$  calculated using helium CR model and a Langmuir probe result.

$7^3\text{D}$  level is the upper limit of the excited levels in the helium CR model, which are treated individually except for levels of the orbital angular momentum quantum number  $L \geq 3$ . For the emission from the  $4^1\text{P}$  state, the Abel transform reproduced a radial profile similar to that obtained from the spectroscopic results, as shown in Fig. 4 (a). In contrast, the Abel transform for more highly excited atoms was inconsistent with the experimental result, as shown in Fig. 4 (b). One possible reason for this discrepancy is the electron temperature used to evaluate  $\varepsilon(y)$ . To perform the Abel transform, the electron temperature and electron density measured by a Langmuir probe were used. However, diagnosis of a low electron temperature plasma using a Langmuir probe has difficulties with anomalous  $I - V$  characteristics [12, 13]. Therefore, the electron temperature obtained by a Langmuir probe,  $T_e^{\text{P}}$ , was substituted with the electron temperature  $T_e^{\text{B}}$  from the Boltzmann plot in the peripheral region, where the emission intensity from highly excited atoms becomes strong. Then, the electron density  $n_e^{\text{P}}$  was also substituted with  $n_e^{\text{B}}$ , which is evaluated using  $T_e^{\text{B}}$  and the electron saturation current. In this report,  $y = 7$  mm was used as a boundary for  $T_e^{\text{P}}$  and  $T_e^{\text{B}}$  because it gives the best-fitted Abel transform result with the experimentally obtained emission intensity profile. The solid line in Fig. 4 (b) shows the result using  $T_e^{\text{B}}$  and  $n_e^{\text{B}}$  for the Abel transform. The calculated profile of the emission intensity from the  $7^3\text{D}$  state developed an emission peak near  $y = 10$  mm. This result also confirms that the low electron temperature plasma localized at the periphery of the plasma column surrounds hot ionizing plasma. The reaction rate of volumetric recombination depends on the electron temperature and electron density. Although the electron temperature was almost constant at around  $-10$  mm  $\leq y \leq 10$  mm, the electron density peaks in the peripheral region, as shown in Sec. 4. Therefore, one possible reason for edge-localized recombining plasma formation is the electron density distribution. Although the Abel transform result was greatly improved by using  $T_e^{\text{B}}$  and  $n_e^{\text{B}}$ , the

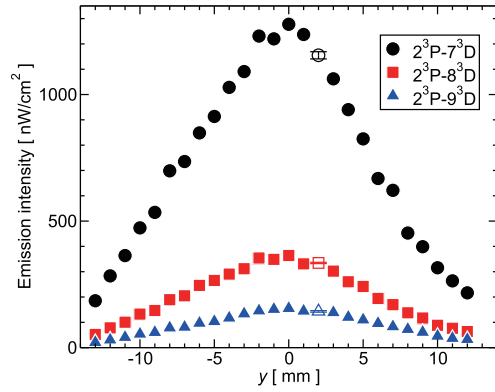


Fig. 5 Radial distribution of the emission intensities from  $2^3P - n^3D$  transitions measured at  $y = 1.43$  m. RF heating power and neutral pressure were approximately  $P_{RF} \sim 350$  W,  $p_{test} \sim 6$  Pa, respectively.

emission intensities obtained by each methods still differ around  $y = 10 - 15$  mm. For the Abel transform, the number of measurement positions along the  $y$ -direction was important because  $\varepsilon(y)$  is obtained using  $T_e^p$  and  $n_e^p$ . Therefore, one possible reason for the difference between the circles and solid line in Fig. 4(b) is insufficient Langmuir probe diagnostics.

### 3.2 Lower RF heating power and higher neutral pressure case (case II)

Helium volumetric recombination was also investigated using a moderate RF heating power and higher neutral pressure, namely,  $P_{RF} \sim 350$  W,  $p_{test} \sim 6.0$  Pa. Figure 5 shows the radial distribution of the emission intensity due to the  $2^3P - n^3D$  ( $n = 7 - 9$ ) transitions. Emission intensity profiles from the transitions shown in Fig. 5 have a peak at  $y = 0$  mm, in contrast to those in Fig. 3. In this plasma production case, the results indicate that volumetric recombination was widely enhanced inside a cylindrical plasma. The radial distribution of a recombination plasma is quite important for energetic ion injection experiments because volumetric recombination is required on the ion beam axis. To understand recombining plasma formation in the DT-ALPHA device, energy relaxation between electrons and ions was investigated, as described in the following section.

## 4. Discussion

In a relatively high electron temperature plasma, ionization and radiation are the main processes of electron energy loss. On the other hand, in a low electron temperature and high electron density plasma, electrons lose their energy mainly through energy exchange between bulk ions instead of the above processes. Then ions transfer their energy to neutral atoms through charge-exchange interactions and elastic collisions. These indicate that ions have an important role in dissipating electron energy in a low electron temperature and high electron density plasma.

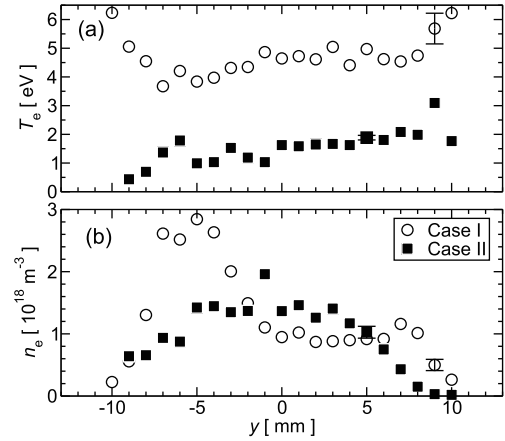


Fig. 6 Radial distribution of (a) electron temperature and (b) electron density measured in the test region using a Langmuir probe for each plasma production case.

The electron-ion temperature relaxation time  $\tau_T^{ei}$  is given as

$$\tau_T^{ei} = \frac{3\sqrt{2}\pi\epsilon_0^2 m_e m_i}{n_i Z_i^2 e^4 \ln\Lambda} \left( \frac{T_e}{m_e} + \frac{T_i}{m_i} \right)^{3/2} \quad (1)$$

where  $m_e$  and  $m_i$  are the mass of the electron and ion, respectively [14, 15].  $Z_i$ ,  $\epsilon_0$ ,  $e$ , and  $\ln\Lambda$  are the ion charge number, permittivity of free space, electron charge, and Coulomb logarithm, respectively. As shown in eq.(1), temperature relaxation between electrons and ions is depends strongly on the electron temperature. The electron temperature and electron density in the test region obtained in each plasma production case using a Langmuir probe are shown in Fig. 6. In plasma production case I, the electron temperature near  $y = 0$  mm was almost uniform at  $T_e \sim 4$  eV and increased to 8 eV toward the edge region, whereas the electron temperature in plasma production case II was  $T_e = 1 - 2$  eV inside the plasma column. Although high electron density plasma,  $n_e > 1 \times 10^{18} \text{ m}^{-3}$ , was achieved in each plasma production case, the radial distributions were quite different. The electron density had a hollowed radial profile that peaked at  $y \sim \pm 7$  mm in plasma production case I, however, the profile became a center-peaked profile in plasma production case II. Then,  $\tau_T^{ei}$  was evaluated using these plasma parameters. Although electron temperature evaluation using a Langmuir probe becomes difficult in low electron temperature plasma where volumetric recombination is strongly enhanced,  $T_e$  and  $n_e$  shown in Fig. 6 were used to approximate  $\tau_T^{ei}$ . Figure 7 shows the radial distribution of  $\tau_T^{ei}/\tau_p$ . Here,  $\tau_p = L/(\alpha C_s)$  corresponds to the plasma particle confinement time in the test region, where  $L$  and  $C_s$  are the characteristic length of the test region,  $L \sim 0.15$  m, and ion sound velocity,  $C_s = (k_B T_e / m_i)^{1/2}$ , respectively. The axial ion Mach number was assumed to be  $\alpha = 0.1$  because directional Langmuir probe measurements have indicated that the axial ion Mach number in the DT-ALPHA device is approximately 0.1 [16]. In plasma production

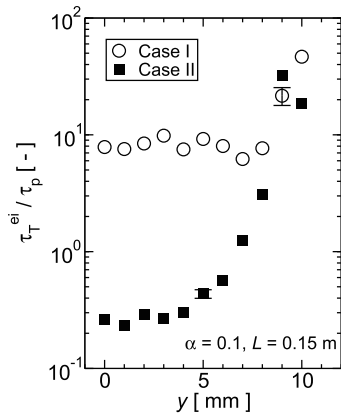


Fig. 7 Radial distribution of the electron-ion temperature relaxation time  $\tau_T^{ei}$  divided by the plasma confinement time  $\tau_p$  in the test region assuming an axial ion Mach number of  $\alpha = 0.1$ .

case I,  $\tau_T^{ei}$  is much larger than  $\tau_p$  around the plasma column. This indicates that electrons escape from the test region before transferring their energy to ions. On the other hand,  $\tau_T^{ei}/\tau_p$  becomes extremely small inside the cylindrical plasma column in plasma production case II. This indicates that electrons rapidly dissipate their energy in the test region while they remain in it. As written in eq. (1),  $\tau_T^{ei}$  depends strongly on  $T_e^{3/2}$ . Thus, reducing  $T_e$  decreases  $\tau_T^{ei}$ , so electron energy transfer is further enhanced. Therefore, volumetric recombination could be enhanced by this feedback. Such results are consistent with the recombining plasma formation shown in Figs. 3 and 5. Electron energy loss due to energy relaxation between ions depends on the  $k(T_e - T_i)$ , where  $k$  represents the electron-ion temperature relaxation coefficient. Therefore, the ion temperature  $T_i$  also becomes important for recombining plasma formation. The ion temperature in the test region could depend on the plasma properties in the production region. Then,  $\tau_T^{ei}$  near the RF antenna was also investigated using a Langmuir probe installed at  $z = 0.98$  m, and the result is shown in Fig. 8. Here,  $L = 0.15$  m and  $\alpha = 0.1$  were also used to evaluate  $\tau_T^{ei}/\tau_p$ . In the plasma production case II,  $\tau_T^{ei}/\tau_p$  near the plasma production region becomes much larger than that in plasma production case I. This indicates that the ion temperature in the test region in plasma production case II decreases because energy transfer to bulk ions is suppressed. In a low electron temperature and high electron density plasma,  $T_e - T_i$  becomes important for electron energy dissipation, so lower  $T_i$  enhances energy transfer from electrons to ions and consequently results in reduction of  $T_e$ . These results confirm that plasma production case II is preferable for recombining plasma formation in terms of electron energy transfer, which is consistent with the spectroscopic results for a recombining plasma (Figs. 3 and 5). However, the ion temperature for each plasma production case was not obtained. Ion temperature diagnostics are expected to yield a more detailed understanding of

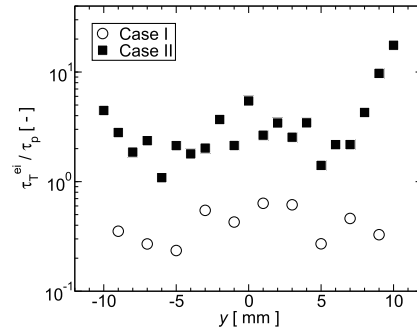


Fig. 8 Radial distribution of electron-ion temperature relaxation time  $\tau_T^{ei}$  divided by the plasma confinement time  $\tau_p$  near plasma production region  $z = 0.98$  m.

helium recombining plasma formation in the DT-ALPHA device.

## 5. Summary

The spatial distribution of helium volumetric recombination in the RF plasma source DT-ALPHA was investigated in two plasma production cases. The radial distribution of the emission intensities from the  $2^3P - n^3D$  transitions was investigated using spectroscopic measurement. It was revealed that at a higher RF heating power and lower neutral pressure, volumetric recombination is strongly localized in the peripheral region of the cylindrical plasma. On the other hand, volumetric recombination was widely distributed around the plasma column at a lower RF heating power and higher neutral pressure case. To understand helium volumetric recombining plasma formation, the electron-ion temperature relaxation time  $\tau_T^{ei}$  was evaluated. In the former plasma production case,  $\tau_T^{ei}$  in the test region was much larger than the plasma confinement time  $\tau_p$ . In contrast, in the latter case,  $\tau_T^{ei}$  became much smaller than  $\tau_p$ , which indicates that electrons lose their energy rapidly while they remain in the test region. The electron-ion temperature relaxation time and plasma confinement time near the plasma production region were also evaluated for each plasma production case.  $\tau_T^{ei}/\tau_p$  was much larger in the latter plasma production case than in the former case. This result indicates that volumetric recombination is enhanced more in the latter case because lower temperature ions enhance the electron temperature reduction, which is consistent with the spectroscopic results. Ion temperature diagnostics are expected to confirm the role of energy transfer to ions in recombining plasma formation in the DT-ALPHA device.

## Acknowledgment

The work is partly supported by Japan Society for the Promotion of Science (JSPS) Grants-in-Aid for Scientific Research (KAKENHI), grant numbers 22740357 and 26420848, and by a Grant-in-Aid for JSPS Fellows, grant number 264331.

- [1] W.L. Hsu, M. Yamada and P.J. Barrett, *Phys. Rev. Lett.* **49**, 1001 (1982).
- [2] N. Ohno, D. Nishijima, S. Takamura, Y. Uesugi, M. Motoyama, N. Hattori, H. Arakawa, N. Ezumi, S. Krasheninnikov, A. Pigarov and U. Wenzel, *Nucl. Fusion* **41**, 1055 (2001).
- [3] Y. Uesugi, N. Hattori, D. Nishijima, N. Ohno and S. Takamura, *J. Nucl. Mater.* **290-293**, 1134 (2001).
- [4] A. Okamoto, H. Takahashi, S. Kitajima and M. Sasao, *Plasma Fusion Res.* **6**, 1201153 (2011).
- [5] A. Okamoto, H. Takahashi, Y. Kawamura, A. Daibo, T. Kumagai, S. Kitajima and M. Sasao, *Plasma Fusion Res.* **7**, 2401018 (2012).
- [6] H. Takahashi, A. Okamoto, Y. Kawamura, T. Kumagai, A. Daibo and S. Kitajima, *Fusion Sci. Technol.* **63**, 404 (2013).
- [7] A. Daibo, A. Okamoto, H. Takahashi, T. Kumagai, T. Takahashi, S. Tsubota and S. Kitajima, *Rev. Sci. Instrum.* **85**, 02B307 (2014).
- [8] H. Takahashi, A. Okamoto, T. Takahashi and S. Kitajima, *Fusion Sci. Technol.* **68**, 190 (2015).
- [9] A. Okamoto, K. Iwazaki, T. Isono, T. Kobuchi, S. Kitajima and M. Sasao, *Plasma Fusion Res.* **3**, 059 (2008).
- [10] T. Fujimoto, *J. Quant. Spectrosc. Radiat. Transfer* **21**, 439 (1979).
- [11] M. Goto, *J. Quant. Spectrosc. Radiat. Transfer* **76**, 331 (2003).
- [12] N. Ezumi, N. Ohno, K. Aoki, D. Nishijima and S. Takamura, *Contrib. Plasma Phys.* **38**, 31 (1998).
- [13] E. M. Hollmann, C. Brandt, B. Hudson, D. Kumar, D. Nishijima and A. Yu. Pigarov, *Phys. Plasmas* **20**, 093303 (2013).
- [14] N. Ezumi, S. Mori, N. Ohno, M. Takagi, S. Takamura, H. Suzuki and J. Park, *J. Nucl. Mater.* **241-243**, 349 (1997).
- [15] D. Nishijima, N. Ezumi, K. Aoki, N. Ohno and S. Takamura, *Contrib. Plasma Phys.* **38**, 55 (1998).
- [16] T. Kumagai, A. Okamoto, H. Takahashi, A. Daibo, T. Takahashi, S. Tsubota and S. Kitajima, *JPS Conf. Proc.* **1**, 015043 (2014).